Disorder-induced phase coexistence in bulk doped manganites and its suppression in nanometer-sized crystals: The case of $La_{0.9}Ca_{0.1}MnO_3$

E. Rozenberg,[1,*] A. I. Shames,[1] M. Auslender,[2] G. Jung,[1] I. Felner,[3] Jaivardhan Sinha,[4] S. S. Banerjee,[4] D. Mogilyansky,[5] E. Sominski,[6] A. Gedanken,[6] Ya. M. Mukovskii,[7] and G. Gorodetsky[1]

[1]*Department of Physics, Ben Gurion University of the Negev, P.O. Box 653, Beer-Sheva 84105, Israel*

[2]*Department of Computers and Electrical Engineering, Ben Gurion University of the Negev, P.O. Box 653, Beer-Sheva 84105, Israel*

[3]*The Racah Institute of Physics, The Hebrew University, Jerusalem 91904, Israel*

[4]*Department of Physics, Indian Institute of Technology, Kanpur, U.P.-208016, India*

[5]*Institute of Applied Research, Ben Gurion University of the Negev, P.O. Box 653, 84105 Beer Sheva, Israel*

[6]*Department of Chemistry and Kanbar Laboratory for Nanomaterials at the Bar-Ilan University Center for Advanced Materials and Nanotechnology, Bar-Ilan University, Ramat-Gan 52900, Israel*

[7]*Moscow Steel and Alloys Institute, Leninskii prospekt 4, Moscow 119049, Russia*

(Received 10 March 2007; revised manuscript received 2 November 2007; published 26 December 2007)

X-band electron magnetic resonance together with dc and ac magnetic measurements were employed for comparative study of magnetic ordering in bulk and nanometer-sized $La_{0.9}Ca_{0.1}MnO_3$ single crystals. A dramatic difference between bulk crystal showing mixed magnetic state, constituted by coexisting canted antiferromagnetic *A*-type matrix and nanometer sized ferromagnetic clusters, and the nanocrystalline form of the same compound, showing mainly ferromagnetic ordering, has been revealed. The complementary study of the structural state and analysis of the electron paramagnetic resonance data in terms of the proposed theoretical model have enlightened the reasons for the observed difference in the magnetic order. The results suggest that the change in magnetic order has an intrinsic nature and is not induced by nonstoichiometry. The cation composition and the oxygen stoichiometry of bulk and nanosized crystals were determined to be the same within the experimental accuracy. Nanometer-sized crystals of $La_{0.9}Ca_{0.1}MnO_3$ are characterized by better chemical and crystalline homogeneity arising both from different fabrication techniques and reduced crystallites size. This effect induces a transition from an inhomogeneous confined state of charge carriers in chemically disordered bulk crystal to a more mobile one in an impuritylike band in homogeneous nanocrystals, resulting in the change of magnetic ordering. A realistic model describing size assisted change of magnetic order in doped manganites has been proposed to interpret the data. The experimental results and their analysis indicate that a chemical/magnetic disorder has a strong impact on the magnetic state and the phase diagram of doped manganites.

DOI: 10.1103/PhysRevB.76.214429 PACS number(s): 76.50.+g, 71.30.+h, 75.47.Lx

I. INTRODUCTION

It is generally accepted that existence of a rich variety of magnetic, electronic, and structural phases, characteristic for doped mixed valence manganite perovskites $R_{1-x}A_xMnO_3$ (R=La and rare earths, A=Ca, Sr, Ba, etc.), is due to a close interplay between charge, spin and lattice degrees of freedom.[1] The ferromagnetic (FM) double exchange (DE) Mn^{3+}-O-Mn^{4+} competes with antiferromagnetic (AFM) superexchange (SE) interaction Mn^{3+}-O-Mn^{3+} between the t_{2g} local spins, as well as with the intersite exchange interaction between e_g orbitals (orbital ordering), spin-lattice interaction, etc. This leads to the coexistence of spatially inhomogeneous phases with different magnetic/electronic order.[1,2] Existing theoretical models predict that spontaneous electronic phase separation (PS) arises from a competition between AFM and FM interactions. Alternatively, PS may be induced by quenched disorder and strains. Spontaneous PS appears as nanometer-scale inhomogeneities,[2] while disorder or strain induced PS shows out on the length scale up to the micrometer range.[3,4] Note that doped manganites are characterized by a chemical and magnetic disorder associated with the doping inhomogeneity. Nevertheless, the simplified theoretical models of DE in manganites mostly ignore such effects. This approach has been recently shown to be inadequate, and the combined action of chemical/magnetic disorder[5] and multiband structure[6] should be included in the DE models. In this context the recent large scale computational model which includes SE interaction and considers competition between FM and charge ordered (CO) nanoscale sized states in doped manganites seems to be more realistic.[7]

Micrometer-scale domains with different electronic density and different magnetic order were observed experimentally in numerous bulk and thin film samples of doped manganites, see, e.g., Refs. 8–10. At the same time, recent improvements of experimental techniques allowed for observations of nano-sized insulating and metalliclike domains in FM-ordered manganite thin film.[11] Their existence was associated with inherent inhomogeneities such as, e.g., local stress. The progress in the thin film preparation methods allowed for fabrication of a unique sample of optimally Ca-doped $La_{0.75}Ca_{0.25}MnO_3$, characterized by an unusual *A*-site La-Ca ion ordering.[12] The ordering compensates the cation mismatch stress already within one supercell, i.e., within the range of ~1.55 nm, leading to an enhancement of electronic homogeneity, suppression of PS-like state, and notable improvement of the macroscopic magnetic/transport properties. These facts direct one to recognize that the structural/

chemical and electronic homogeneity on the nanoscale range are the necessary prerequisites for understanding the internal regularities governing the properties of doped manganites. On the other hand, almost all practical samples contain unavoidable structural imperfections, chemical disorder, and associated strains.[13] Thus, a basic question arises about the extent to which the experimentally observed complex multiphase behavior can be described by the simplified DE models neglecting the chemical and magnetic disorder, as well as the appearance of impurity bands.[2–4]

Let us consider $La_{0.9}Ca_{0.1}MnO_3$ (LCMO) manganite compound as an example. The literature data concerning its magnetic ordering are strongly contradictive. The neutron diffraction and magnetic measurements on bulk crystals of LCMO reveal modulated canted AFM structure composed of *A*-type canted AFM matrix and nanometer-scale FM clusters.[14,15] In a marked contrast, low temperature coexistence of major FM and minor canted AFM insulating phases was reported for bulk LCMO crystal in Ref. 16. The neutron and high-resolution x-ray powder diffraction, as well as ac/dc magnetic measurements show only the homogeneously canted AFM phase in the stoichiometric LCMO ceramic.[17] On the other hand, it was suggested in Refs. 18 and 19 that the nanosized FM metalliclike clusters are embedded into the FM insulatinglike matrix in LCMO bulk ceramics. It seems, therefore, that the basic question whether the extrinsic or intrinsic reasons are responsible for appearance of coexisting magnetic/electronic phases in LCMO, as well as the question on the applicability of the simplified models[2–4] may be addressed to this very case.

It is well known that finite-size effects induce a plethora of new phenomena in the solid state magnetism.[20,21] In particular, it is believed that the reduction of the sample size down to the nanometer size scale is capable of influencing the magnetic ordering in doped manganites via the coupling between the spin subsystem (spins of both Mn ions and carriers) and the lattice. Recent experiments showing FM like ordering in crystalline $Pr_{0.5}Ca_{0.5}MnO_3$ nanowires[22] and $Nd_{0.5}Ca_{0.5}MnO_3$ nanoparticles[23] in a marked difference to the observations of the AFM charge ordered ground state in the bulk crystalline form of these manganites, were interpreted as an evidence of the suppression of the AFM/CO state in nanosized samples. The actual mechanism of this suppression is currently a subject of a discussion.[22,23] Additionally, a progressive increase of low temperature, low field magnetization with decreasing mean grain size in $LaMnO_3$ nanoparticles was reported in Ref. 24. These experimental findings strongly support a claim that the reduction of sample size influences magnetic ordering in doped manganites.

In this paper, we report on a comprehensive study of the crystalline structure and magnetic ordering in bulk and nanosized $La_{0.9}Ca_{0.1}MnO_3$ manganite single crystals. The studies were performed in order to obtain additional experimental insight into the problem of complex multiphase behavior of LCMO by benefiting from a special advantage of using the homogeneous nanometer sized samples as the reference ones. The notable difference in chemical and structural homogeneity between the bulk and nanometer sized crystals of the same $La_{0.9}Ca_{0.1}MnO_3$ composition arises from different fabrication protocols employed. For probing the magnetic ordering we have used the electron magnetic resonance (EMR) technique, comprising the electron paramagnetic resonance (EPR) and the ferromagnetic resonance. High sensitive EMR method allows one to detect small changes of the magnetic homogeneity induced by the local variations of the oxygen stoichiometry and chemical composition.[25] Independent ac and dc magnetic data complemented the EMR results. It was clearly shown that the stoichiometry of low-doped $La_{1-x}Ca_xMnO_3$ ($x \leqslant 0.20$) manganites determines their magnetic ordering.[17,26] Therefore, special attention was paid to the chemical composition and stoichiometry of our samples. We have assured that not only the chemical composition, but also the oxygen stoichiometry of the investigated bulk and nanosized LCMO were the same. We believe that our approach is much more appropriate than the one reported in Refs. 22 and 23 where only the composition and stoichiometry of nanomanganites were concerned.

To draw conclusions about the magnetic correlations and spin dynamics in the investigated samples the EMR parameters at the paramagnetic (PM) temperature range were analyzed using the existing models.[27–29] This allowed us to evidence a notable difference in the features of Jahn-Teller transition and in the magnetic ordering in nanosized $La_{0.9}Ca_{0.1}MnO_3$ and in its bulk counterpart. We believe that a higher chemical homogeneity of the nanometer-sized crystals leads to their basically FM ordering in a marked contrast to the mixed AFM+FM order in the bulk crystals. We attribute the difference in the magnetic order to a transition from an inhomogeneous confined state of charge carriers in the chemically/magnetically disordered bulk crystal to a more mobile one within impuritylike band[5] in homogeneous nanocrystals. The change in the electronic states and in the magnetic ordering seems to be an intrinsic one and not induced by differences in the chemical composition or oxygen stoichiometry between the bulk and nanosized LCMO. This fact motivated us to propose a model describing the influence of the chemical/magnetic disorder suppression associated with the size reduction upon magnetic order in doped manganites. The proposed model explains not only our experimental results but also those reported previously for $Pr_{0.5}Ca_{0.5}MnO_3$ and $Nd_{0.5}Ca_{0.5}MnO_3$ compounds.[22,23] Our results may therefore help to fill the gap between the idealized models[2–4] and numerous experiments evidencing the phase coexistence in doped manganites.

II. EXPERIMENT

Bulk LCMO crystals were grown by a radiative heating floating-zone method.[30] Nanocrystals were prepared by the sonication-assisted coprecipitation and subsequent low temperature crystallization at 900 K,[31] i.e., below the temperature of its structural rhombohedral to orthorhombic transition.[32] Such nanocrystals fabrication procedure effectively eliminates twin defects, reduces stoichiometry fluctuations, and renders the samples almost free from extended defects and associated local strains, leaving the crystallite surface as the only dominant defect. The structure of the nanocrystals was checked using JEM 2010 high resolution transmission electron microscope (TEM) with the linear

resolution of 1.9 Å. X-ray diffraction (XRD) measurements were carried out with the Huber Imaging Plate camera installed on an Ultrax 18-Rigaku X-ray rotating Cu anode source. The Rietveld refinement of the XRD data was performed using the FULLPROF program.[33] The cation composition of the nano and bulk LCMO was additionally examined by the electron dispersive x-ray analysis and inductively coupled plasma atomic emission spectroscopy techniques and was found to be La/Ca/Mn=0.9/0.1/1.0, the same in the bulk and nanosystem within the experimental accuracies of 0.01.

The EMR measurements were performed with Bruker EMX-220 X-band (ν=9.4 GHz) spectrometer in the temperature range 5 K$\leqslant T\leqslant$600 K using small amounts (few mg) of fine powdered samples. The bulk crystal was crushed up to the micron-sized (5–20 μm grains) powder, while the nanocrystalline sample was measured in the as fabricated state. The loose-packed form of the powder samples enables one to exclude the influence of the skin effect[25,34] and to narrow the signals in the FM state, due to the texture of fine particles in the external magnetic field. This, in turn, gives one an opportunity to examine a complex EMR signal in more details. In the course of the experiments we have analyzed the temperature dependences of the following EMR spectra parameters: the resonance field H_r, peak-to-peak line width ΔH_{pp} and the doubly integrated intensity (DIN), which is proportional to the EMR susceptibility χ_{EMR}. The temperature and the magnetic field (H) dependences of dc magnetization M were measured using a SQUID magnetometer in the temperature range of 5–300 K and under H up to 5 T. ac susceptibility (χ) measurements were carried out with the homebuilt setup at the external H_{dc}=5 Oe and the exciting H_{ac}=2 Oe.

III. RESULTS AND DISCUSSION

A. Structural state of the nano and bulk LCMO

The room temperature XRD spectra for both samples are presented in Fig. 1. The respective x-ray peaks of the nano crystals are broadened compared to the bulk ones, but nevertheless, both spectra show the same single-phase nature of the samples studied. On the basis of the Rietveld method, both specimens can be structurally described by the orthorhombic P_{nma} space group. The lattice parameters: a=5.465 Å, b=7.739 Å, c=5.506 Å and a=5.5932 Å, b=7.730 Å, c=5.5276 Å, as well as the unit cell volumes of 232.9 Å^3 and 238.9 Å^3 were obtained for the nano and bulk crystals, respectively. The nanocrystals' unit cell turns out to be compressed when compared to the bulk one, while the bulk unit cell volume is very close to that of the stoichiometric LCMO ceramics.[26] Moreover, the characteristic relations between the lattice parameters in P_{nma} notation: $c\geqslant a\geqslant b/\sqrt{2}$ (O* symmetry) and $a>c>b/\sqrt{2}$ (O$'$ symmetry)[17,26] are fulfilled for the nano and bulk crystals, respectively. As a result, splitting of (101) and (020) XRD peaks is absent (reduced orthorhombic distortions) in the nano LCMO, see inset to Fig. 1(a), while such splitting is clearly visible in the bulk LCMO x-ray spectrum, i.e., in the inset to Fig. 1(b). The orthorhombicity of the nano LCMO is confirmed by the weak peaks at 2θ=25.6° and 54.2° which can be indexed as (111) and (113,331) XRD lines. These lines are characteristic for the P_{nma} symmetry and are not observed at these angles in close cubic or rhombohedral symmetries. The relationship between the structural features of nano and bulk crystals and their electronic/magnetic ordering is discussed in detail later.

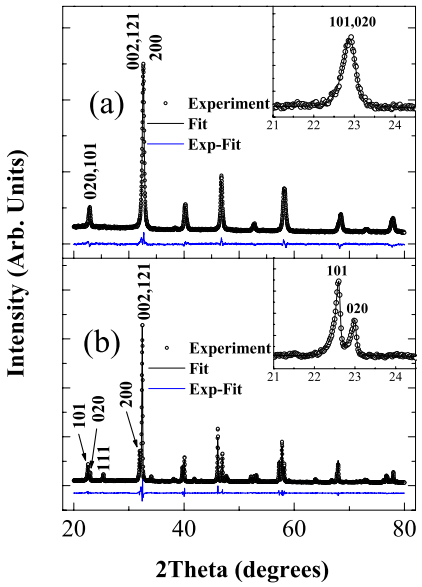

FIG. 1. (Color online) Observed (dots) and Rietveld fitted (lines) room temperature x-ray diffraction patterns for crystalline $La_{09}Ca_{0.1}MnO_3$ samples: (a) Nanometer-sized (R_{wd}=6.2%) and (b) bulk crystals (R_{wd}=9.6%). Insets: The magnified view of the patterns near (101) and (020) reflections.

The crystallinity of the nanosample was additionally checked by the high resolution TEM. As shown in Fig. 2, it is perfect for both individual, Fig. 2(a), and agglomerated, Fig. 2(b), nanograins. Extended structural defects (dislocations, twins, etc.) characteristic for the bulk form of manganite crystals[13] were not found in our nanocrystals. The average size of the nanograins was determined by means of XRD and TEM techniques and found to be of 24±4 nm.

B. Magnetic and resonance properties of the nano and bulk LCMO

The temperature dependences of magnetization $M(T)$ measured at the low field of 5 Oe after zero-field (ZFC) and field-cooling (FC) procedures are shown in Figs. 3(a) and 3(b) for bulk and nano LCMO, respectively. In the bulk sample FC and ZFC $M(T)$ curves split below $T\sim$130 K go through a pronounced maximum at $T\sim$112 K and cease to change significantly below 70 K. In contrast, in the nanosample ZFC and FC $M(T)$ curves are separated already at $T\sim$240 K. The FC magnetization increases down to 5 K, while ZFC magnetization demonstrates a broad maximum at $T\sim$90 K. Note that similar long $M(T)$ tails have been previously observed in nanopowders of LCMO with average particle size ~11 nm.[35] The characteristic temperatures of the bulk crystal, $T\sim$130 K and $T\sim$112 K, are marked by clear maxima in the temperature dependence of the real part of ac

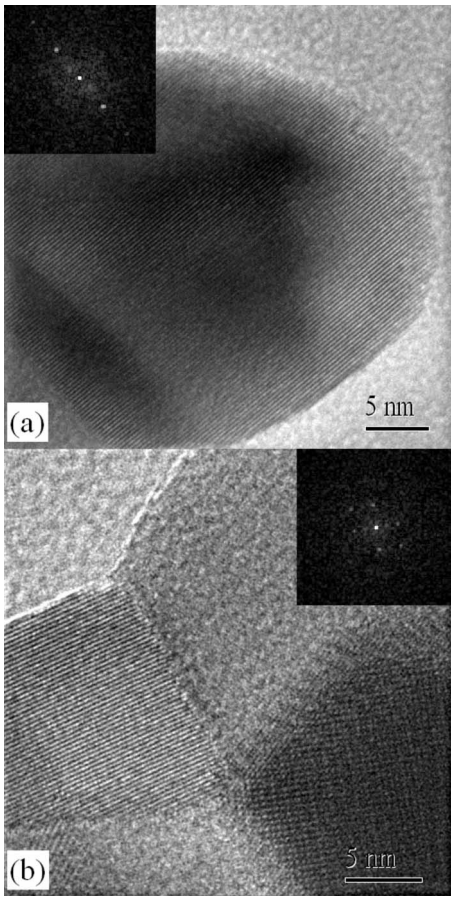

FIG. 2. HRTEM image of (a) individual and (b) agglomerated $La_{0.9}Ca_{0.1}MnO_3$ nanograins. The lattice fringes correspond (a) to the (200) plane and (b) to (101)+(020) planes. Insets: The fast Fourier transform patterns of these planes.

susceptibility $\chi'(T)$ shown in Fig. 3(c). χ' of a nanocrystal exhibits a broad maximum in the vicinity of 90 K and a long tail extending up to 240 K; see Fig. 3(d). The susceptibility is frequency dependent in the temperature range 5–240 K and 60–130 K for the nano and bulk samples, respectively. Note that only the temperature anomalies in $\chi'(T)$ curves were used for characterization of the magnetic ordering in nano and bulk LCMO. For this reason, the arbitrary units are used in Figs. 3(c) and 3(d).

The magnetic field dependence of magnetizations $M(H)$ measured after ZFC is shown in Fig. 4(a). The magnetic response of both samples at low temperatures (5 K) is FM like, but their $M(H)$ are not saturated at the magnetic field up to 5 T. Spontaneous magnetization M_0 was found to be 2.44±0.04 and 2.20±0.01 μ_B/f.u. for bulk and nano LCMO, respectively. Such difference between M_0 values seems to result from low-temperature freezing of the FM clusters moments in strong field of AFM anisotropy in bulk LCMO and from the interplay between magnetic disorder at the nanosurfaces and interparticle interactions, as well as the appearance of FM ordering in the cores of nanograins, as discussed in detail later. With the increasing temperature the bulk $M(H)$ dependence becomes linear and M_0 disappears at Curie temperature (T_C), as expected for a PM state. In contrast, the

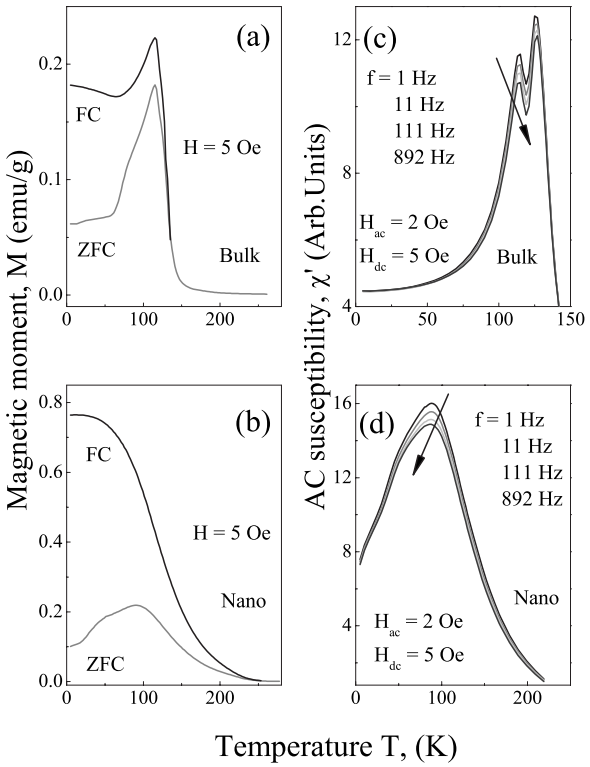

FIG. 3. Temperature dependence of field-cooled and zero-field-cooled magnetization of (a) bulk and (b) nanosample at H=5 Oe. Temperature dependence of the real part of ac susceptibility in (c) bulk crystal and in (d) nanosample.

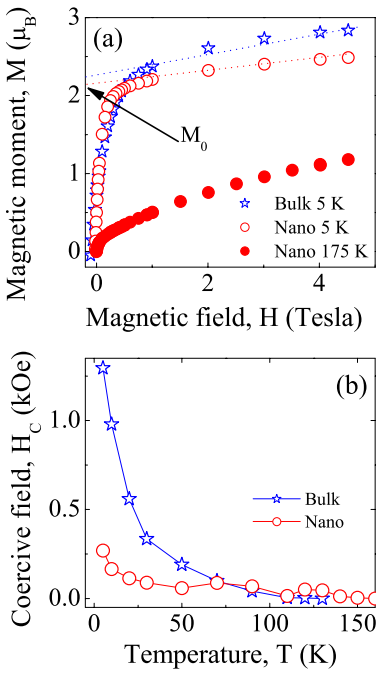

FIG. 4. (Color online) (a) dc magnetic field dependence of the magnetization of the bulk at T=5 K and of the nanocrystalline sample at 5 and 175 K. (b) Temperature dependence of the coercive field.

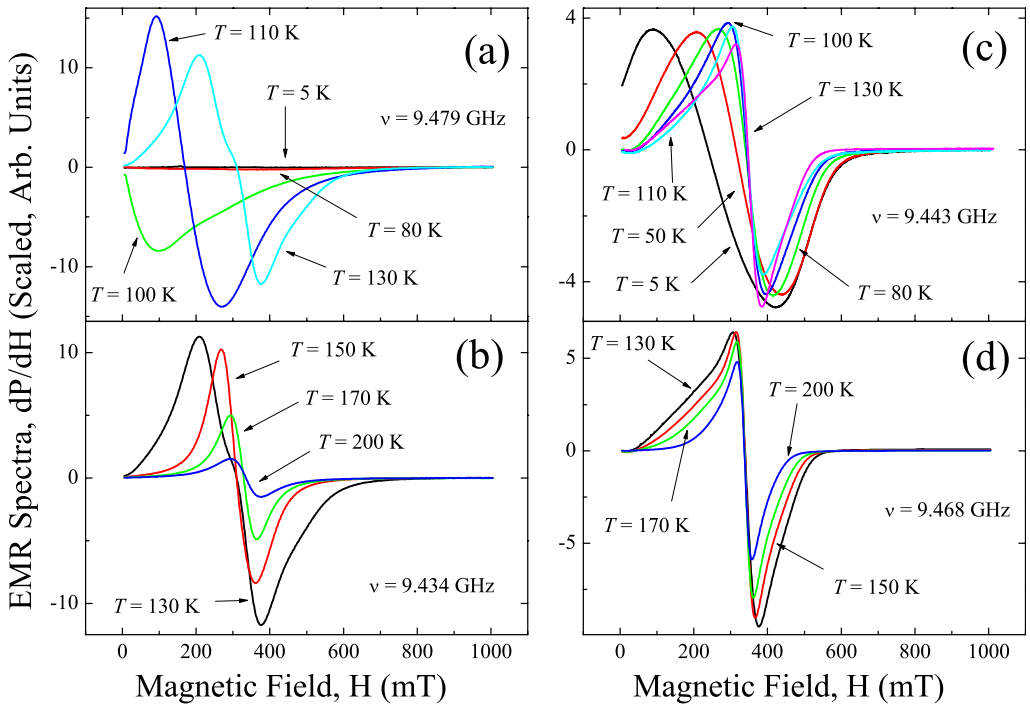

FIG. 5. (Color online) EMR spectra of (a), (b) bulk and (c), (d) nanocrystalline samples recorded at different temperatures above and below magnetic transition points.

nonlinear, nonhysteretic, and nonsaturated $M(H)$ curves are recorded for nanosamples between 150 K and 240 K; see Fig. 4(a). The coercive field H_C decreases with increasing temperature and vanishes around 150 K in the nanocrystal, and around 130 K in the bulk—Fig. 4(b).

The results of the magnetization and susceptibility measurements (Figs. 3 and 4) of the LCMO bulk crystal are consistent with the existing literature data.[14,15] The magnetic ground state is a modulated canted AFM structure composed of A-type AFM matrix and nanometer-scale FM clusters. There are two subsequent magnetic transitions in the bulk: A FM transition (long range ordering of the FM clusters) at $T_C = 130 \pm 2$ K and an AFM transition of the matrix at Néel temperature $T_{CA} = 112 \pm 1$ K. The magnetic ordering in LCMO nanocrystals is clearly different from the one observed in its bulk counterpart.

The EMR data confirm a marked difference in magnetic orderings. EMR detects the power P absorbed by the sample from the transverse magnetic microwave field as a function of the static field H. The signal-to-noise ratio of the spectra is improved by recording the derivative dP/dH. EMR spectra (dP/dH) of the bulk show a single resonance line within the entire temperature range of measurements; see Figs. 5(a) and 5(b), while a complex line appears in the spectra of the nanosample between 115 and 240 K; see Fig. 5(d). Figure 6 shows that this complex line may be simulated/fitted as being composed of a broad Gaussian and a narrow Lorentzian line. The doubly integrated EMR intensity (DIN) of the bulk sample starts to increase with decreasing temperature at $T \sim 175$ K, reaches a maximum at $T_{max} = 125$ K and practically vanishes below 90 K; see Fig. 7(a). The vanishing of DIN reflects directly the zeroing of the resonance signal in bulk LCMO, as shown in Fig. 5(a). In contrast, DIN of the nanosample starts to increase already at $T = 250$ K and grows monotonically towards a weak maximum at $T \sim 20$ K.

Temperature dependences of the resonant linewidth (ΔH_{pp}) are shown in Fig. 7(b). The $\Delta H_{pp}(T)$ of the bulk goes through a broad minimum at $T = 420$ K, well pronounced minimum at $T = 175$ K, and a subsequent increase until the EMR signal becomes unobservable around 115 K. In the nanosample the $\Delta H_{pp}(T)$ sharply decreases in the vicinity of 500 K which is close to the temperature of the LCMO Jahn-Teller (JT) transition; see Ref. 36, and references therein. The narrowing of the EMR linewidth in the vicinity of JT transition was reported, e.g., in Ref. 37. Upon further cooling the $\Delta H_{pp}(T)$ goes through a broad minimum at $T \sim 250$ K

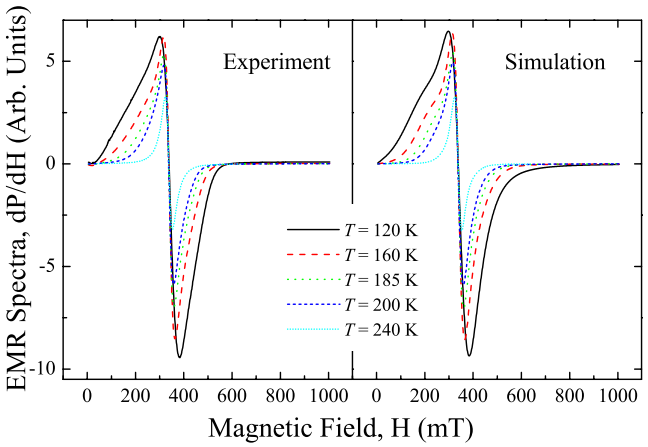

FIG. 6. (Color online) EMR spectra of nanocrystalline LCMO recorded at the temperature interval of two magnetic phase coexistence and its simulation with a broad Gaussian and a narrow Lorentzian contribution.

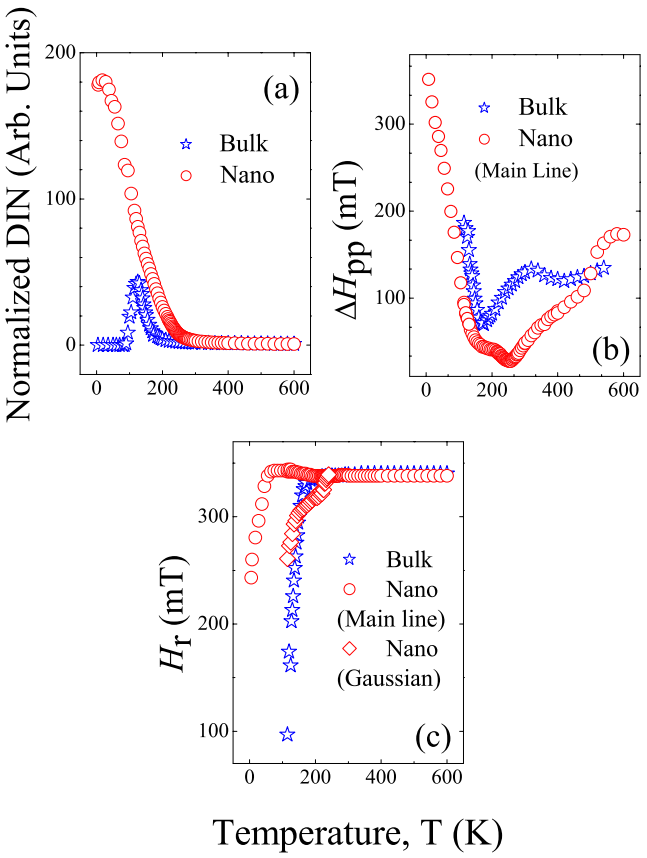

FIG. 7. (Color online) Temperature dependences of the EMR parameters for the bulk and nanocrystalline $La_{0.9}Ca_{0.1}MnO_3$ samples. (a) Doubly integrated intensity of the signal. (b) Linewidth. (c) Resonance fields.

and then increases down to the lowest temperatures. Let us emphasize that JT-like transition is clearly seen in the ΔH_{pp} of nanocrystals, while in the bulk crystal only a broad minimum at 420 K is observed—Fig. 7(b).

Temperature dependences of the resonance fields H_r for all extracted signals are shown in Fig. 7(c). In the far PM region H_r is T-independent and close to 340 mT, corresponding to the PM g factor of 1.99 ± 0.01 for both samples. H_r of the bulk decreases sharply below 190 K, while for nanosample the H_r of broad Gaussian and main Lorentzian EMR lines decrease relatively slow below 220 K and 75 K, respectively; see Fig. 7(c). Deviation of H_r from its PM value is caused by anisotropic spin-spin interactions and net magnetization appearing due to long- or short-range FM correlations when T decreases towards T_C. The 175 K minimum in $\Delta H_{pp}(T)$ and a decrease of H_r below 190 K can thus be seen as a hallmark of the formation of short-range FM correlated clusters in the bulk crystal at $T>T_C$.[38,39] The appearance of AFM ordering at $T<T_{CA}$ broadens EMR signal and strongly decreases its intensity and H_r. At low temperatures where the AFM order dominates, the X-band EMR becomes unobservable in the bulk LCMO; see Figs. 5 and 7.

The existence of the two superimposed EMR signals, as well as a different behavior of their $\Delta H_{pp}(T)$ and $H_r(T)$, see Figs. 6 and 7(c), indicate that in the nanocrystals an additional magnetic phase coexists with the PM one below 240 K. The weak Gaussian line can be resolved only at the temperatures where nonlinear, nonhysteretic, and nonsaturated $M(H)$ dependences, characteristic for a superparamagnetic (SPM) system, are observed. The existence of a broad maximum in ZFC $M(T)$ of a nanosample in Fig. 3(b) can be associated with the blocking effects in a SPM system in which each nanoparticle possesses a spontaneous magnetic moment. However, the classical blocking temperature is expected to increase with increasing H, while in our case the ZFC $M(T)$ maximum completely disappears already at applied fields of a few G. Since the temperature $T\sim90$ K of the maximum in ZFC $M(T)$ coincides with the maximum in $\chi'(T)$ and with the temperature of the inflexion point in FC $M(T)$, we associate it with onset of the ferromagnetic ordering in the cores of nanocrystals. The internal field resulting from such ordering decreases H_r in nanocrystals below 75 K; see Fig. 7(c). Note that Ca content $x=0.1\pm0.01$ in the nano LCMO is far from the critical concentration ($x_{cr}=0.125$) marking the FM order onset in bulk $La_{1-x}Ca_xMnO_3$.[14] It allows us to consider this ordering as inherent and specific for the nanoform of LCMO, as elaborated further on.

The existence of the SPM phase may be associated with some high-temperature magnetic ordering in the PM system of nanocrystals, i.e., with the appearance of spin clusters having net magnetic moments. An obvious difference between the nano and bulk sample is a strong influence of surfaces and interparticle interactions on the system properties. Random magnetic ordering of the surface Mn spins and their interactions (e.g., dipole-dipole like) within an ensemble of nanocrystals may lead to the appearance of SPM phase. The broad Gaussian-like EMR signal originating from that phase contributes about 5–7 % to the total EMR intensity. We attribute the origin of this line rather to spin clusters randomly distributed along the surface than to a continuous surface shell. A plausible mechanism for the surface cluster ordering is the tunneling of carriers through junctions formed by the contact points between adjacent nanoparticles. The influence of the surface tunneling on electrical transport in nano-manganites is actively discussed now; see, e.g., Ref. 40. Therefore, it seems reasonable to suggest that the same effect leads to a surface clustering at temperatures below which thermal fluctuations are unable to destroy local FM clusters. Electron tunneling between two Mn ions belonging to different nanocrystal particles,[41] similarly to the electron hopping between two Mn ions in the bulk lattice, induces FM double exchange correlation. The DE correlation over the grain-surface contact is likely stronger than its bulk counterpart due to the dangling of some of the AFM Mn-O-Mn bonds on the surface. As a result, the FM-correlated spin clusters of low concentration appear at the contacting grains interfaces. The spatial frustration of the grains in the agglomerate results in the randomization of FM moments and in the formation the suggested SPM like phase. Upon cooling towards $T_C\sim90$ K this effect starts to compete with the FM ordering in the grains cores and, as a result, the SPM like EMR signal becomes unobservable below 115 K.

The low-temperature system of FM cores and magnetically disordered surfaces in nanocrystals is more homogeneous and less anisotropic than the mixed phase of the

canted AFM matrix and FM clusters coexisting in bulk single crystals. This leads to higher values of low-temperature, high-field differential susceptibility and higher coercive fields in the bulk; see Fig. 4. Frustration of the PM spin subsystem, due to appearance of SPM-like phase in nanocrystals below 240 K, is responsible for the frequency dependent susceptibility. The effect is most pronounced near $T_C \sim 90$ K. Increase in the magnetic anisotropy of nanocrystal below 90 K visibly reduces the frequency influence but does not remove it totally. In contrast, the dominant effect of the AFM matrix in the bulk at low temperatures induces high magnetic anisotropy, freezes FM clusters, and fully eliminates the frequency dependence of $\chi'(T)$ below 60 K, compare Figs. 3(c) and 3(d). At $T > 60$ K the frequency dependence is observed up to the bulk T_C, even if a more sensitive EMR method detects the presence of FM clusters in the PM matrix up to ~190 K.

Let us summarize briefly the experimental data. XRD shows phase purity and the same crystallographic P_{nma} structure for both nanometer-sized and bulk crystalline LCMO. But the different O^* and O' symmetries with reduced and enhanced orthorhombic distortions are characteristic for nano and bulk LCMO, respectively. The crystallinity of nanosample, checked by high resolution TEM, shows no extended structural defects characteristic for the bulk. The same cation composition of both samples was confirmed by the electron dispersive x-ray analysis and inductively coupled plasma atomic emission spectroscopy techniques. The results of ac/dc magnetic and resonance (EMR) measurements, presented in Figs. 3–7, were interpreted in terms of a notable difference between the magnetic ordering in the nano and bulk LCMO. In particular, magnetic ground state of the bulk crystal is a modulated canted AFM structure, composed of the A-type AFM matrix and nanometer-scale FM clusters, consistently with the literature data. In a marked contrast, more homogeneous FM state together with the surface magnetic frustration is characteristic for the nanoform of LCMO crystals. An additional SPM like phase is detected below 240 K, most likely due to the tunneling of carriers through the contacts between surfaces of adjacent nanograins in the agglomerated sample.

To obtain an additional insight into the nature of the magnetic orderings, we have fitted the EPR data of both nano and bulk LCMO to the known theoretical models. The results suggest that a difference in magnetic ground states is a direct consequence of a strong impact of different chemical/magnetic disorder in the nano and bulk forms of the LCMO.

C. Modeling of the electron paramagnetic resonance data for nano and bulk LCMO

In general, the EPR line is a single Lorentzian at temperatures above 190 K in the bulk, and above 240 K in the nanocrystals. The Lorentzian signal is characterized by the same temperature independent PM g factor $g = 1.99 \pm 0.01$ for both samples; see Fig. 7(c). The g-factor value is typical for Mn^{4+} in the $(O^{2-})_6$ octahedron coordination indicating that the majority of e_g electrons leave Mn^{3+} ions and become either itinerant or localized outside the Mn^{4+} ions. It appears that

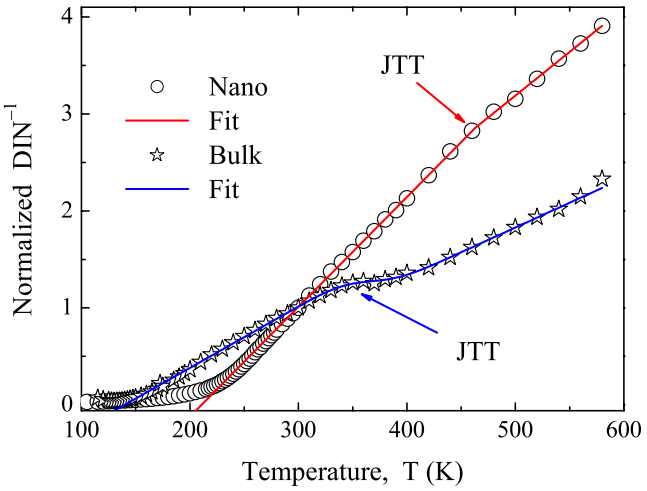

FIG. 8. (Color online) Inverse DIN normalized to its value at 300 K as function of temperature for nanometer-sized and bulk crystals. The fittings were done with Eqs. (1) and (2) as it is described in text. Arrows point out Jahn-Teller transition (JTT).

$$\mathrm{DIN} \propto \chi_{\perp}[T, H_r(T)] = \frac{M[T, H_r(T)]}{H_r(T)}, \quad H_r(T) \gg \Delta H_{\mathrm{pp}}(T), \tag{1}$$

where $\chi_{\perp}(T,H)$ is the transverse susceptibility. Equation (1) shows that DIN is not equivalent to any magnetic susceptibility unless either $H_r(T)$ is constant and/or $\chi_{\perp}(T,H) = \chi(T)$ is field independent. In the far PM range these conditions are fulfilled and the DIN may be considered as being equivalent to EPR susceptibility. The temperature dependence of the inverse DIN normalized to the value at 300 K is shown in Fig. 8. For the nanocrystals, the dependence is fairly piecewise linear. We have fitted the linear dependence to the Curie-Weiss (CW) law, DIN $\propto \chi = C/(T - \Theta)$, using two different Curie constants and Curie-Weiss temperatures C_1, Θ_1 at 300 K $\leqslant T \leqslant T_0$ and C_2, Θ_2 at $T_0 < T < 600$ K, while preserving the χ continuity at $T = T_0$. The fit parameters are presented in Table I. Remarkably, T_0 proves to be close to the temperature $T_{O'\text{-}O^*} \sim 500$ K of the structural transition,[36] which accompanies cooperative JT effect in the bulk LCMO ceramics. However, XRD data for the nano LCMO in Fig. 1(a) show the reduced orthorhombicity, which is usually associated with the absence of the JT transition.[17,26] The spin correlations are FM all over the PM range and the large value of $\Theta(T < T_0)$ is apparently due to the appearance of DE coupling.[2,6] Remember that for a given Ca doping level $\Theta(x)$ is a sum of SE and DE contributions. Using Eq. (29) from Ref. 5, which was obtained for an ideal DE model,[2] we estimate $\Theta_{\mathrm{DE}}(0.1) \approx 135W$ eV^{-1} K, where W is the e_g bandwidth. Taking $\Theta_{\mathrm{SE}}(0) \approx \Theta_{\mathrm{LMO}} = 46$ K,[42] one can estimate that W changes from 1.2 to 0.8 eV upon heating through T_0. The estimated values agree with the theoretical evaluation $W \sim 1$ eV and with the narrowing of the e_g bandwidth expected from the polaron effect above the JT transition point.[2] We conclude that in the nano LCMO only an electronic part of JT effect shows up, while its structural transition counterpart is blocked.

TABLE I. The temperatures of magnetic transitions (T_{CA} is the Néel temperature of the A-type AFM matrix in bulk) and parameters of the DIN^{-1} fit. The parameters are the following: T_0 is the estimated temperature of cooperative/electron Jahn-Teller transition (in the bulk crystal it corresponds to an average Ca content); σ_T is the smearing interval of the above transition (applies to the bulk crystal only); Θ_1 and Θ_2 are the Curie-Weiss temperatures below and above the transition; C_2/C_1 is the ratio of the Curie constants above and below the transition.

Sample	Transition temp. (K)	T_0 (K)	σ_T (K)	Θ_1 (K)	Θ_2 (K)	C_2/C_1
Nano	$T_C \approx 90$	463±6		210±2	145±5	1.26±0.03
Bulk	$T_{CA}=112\pm1$	365±2	32±4	137±2	135±7	1.24±0.03
	$T_C=130\pm2$					

The DIN^{-1} versus T curve for the bulk, shown in Fig. 8, is different from the one recorded with the nanocrystals. Although two CW-like regimes are also observed, the deviation from the piecewise straight line is noticeable and the transition between two regimes has a smeared steplike form. To explain such a behavior we refer to the evidence nonhomogeneous Ca distribution in $La_{1-x}Ca_xMnO_3$ bulk crystals.[43] Let us assume that the Ca concentration is Gaussian distributed with a mean x and dispersion σ_x. Then, for small enough σ_x, the distribution of the structural transition temperatures will also be Gaussian with a mean $T_0=T_{O'\text{-}O^*}(x)$ and the dispersion $\sigma_T=|dT_{O'\text{-}O^*}(x)/dx|\sigma_x$. For the spatially averaged susceptibility, adopting the CW law with different parameters C_1, Θ_1 and C_2, Θ_2 in the O' and O^* phases, respectively, we obtain

$$\chi(T)=\frac{1}{2}\left[1+\mathrm{erf}\left(\frac{T_0-T}{\sigma_T}\right)\right]\frac{C_1}{T-\Theta_1}+\frac{1}{2}\left[1+\mathrm{erf}\left(\frac{T-T_0}{\sigma_T}\right)\right]\frac{C_2}{T-\Theta_2}, \quad (2)$$

where $\mathrm{erf}(z)$ is the error function. Note that Eq. (2) provides an excellent fit for the DIN versus T data for the bulk LCMO, as shown in Fig. 8. The fitting parameters are shown in Table I. T_0 of the bulk is lower than $T_{O'\text{-}O^*}$ for the corresponding ceramic LCMO[36] even taking into account the smearing range $\sim\sigma_T$. Let us emphasize that the ratios of the Curie constants above and below the electronic/structural transition in the nano and bulk LCMO are practically the same, see Table I.

The analysis of the PM spin dynamics, closely related to the analysis of the DIN in the paramagnetic range, is based on the formula employed previously[27] for $La_{1-x}Ca_xMnO_3$ ceramics

$$\Delta H_{pp}(T)=L(T)\chi_0(T)/\chi(T). \quad (3)$$

Here $\chi_0(T)=CT^{-1}$ is the Curie susceptibility, C is the highest temperature Curie constant, and $L(T)$ is a kinetic coefficient. The relation of $L(T)$ to a time correlation function of quantum torques which cause total spin components to relax was discussed in Ref. 27. It was shown that $L(T)$ should saturate very fast at $T \gg \Theta$ if the manganite can be described as a mixture of rigid Mn^{3+} and Mn^{4+} ions. For this case the susceptibility factor in Eq. (3) dominates the temperature dependence of the linewidth in the PM range, which was indeed observed in the ceramic $La_{1-x}Ca_xMnO_3$.[27] The saturation value, $\Delta H(\infty)$ was estimated[27] to be proportional to the Dzialoshinsky-Morya interaction[44,45] and the crystal field[46] strengths squared divided by an effective exchange interaction modulus.

In our samples, in particular in the nano LCMO, the temperature dependence of ΔH_{pp} is not fully consistent with the constant L concept. To account for the ΔH_{pp} at the PM state we assume, on the base of the H_r data from Fig. 7(c), that e_g electrons, even if localized, do not occupy the manganese sites. Following this assumption, the kinetic coefficient may be naturally decomposed into two parts $L=L_{Mn^{4+}}+L_{e_g}$. For the first term, which is due to spin-spin relaxation of Mn^{4+} ions, we still retain the assumption of Ref. 27, viz.

$$L_{Mn^{4+}}(T)=\Delta H_i^{\infty}. \quad (4)$$

The second term is due to the spin relaxation of e_g electrons mediated by various interactions with the lattice imperfections and can be estimated using DE model with potential disorder[5] and a simplest electron-impurity interaction with the spin reversal, which is a reason for broadening of the EPR line in semiconductors.[28] The result for the PM state is

$$L_{e_g}(T)=BTe^{-E_A/kT}, \quad (5)$$

where B is a constant proportional to the spin-orbit coupling squared divided by the e_g band width. The activation energy E_A is the difference between the Fermi energy μ and the e_g-band top. Usually E_A equals full or half the gap between the e_g-band and an acceptorlike impurity band, which emerges due to crystal imperfections and doping.[5] Remarkably, L_{e_g} is proportional to the conductivity estimated within the same model.[29]

For the nanocrystals, ΔH_{pp} at PM state is an increasing function of T and shows a jumplike behavior when approaching T_0. But contrary to the abrupt change of χ, the steplike variation of ΔH_{pp} extends over $\sim$50 K around T_0; cf. Figs. 8 and 9. We have fitted Eqs. (3)–(5) to the ΔH_{pp} data in the temperature range 300 K$\leqslant T \leqslant$460 K$<T_0$. We could not use the entire range of the experimental data, up to 600 K, because of very few data points available above T_0 and the absence of the formula for L in the transition range. The fit shown in Fig. 9 yielded $E_A=0$, indicating the bandlike nature of carriers in the nano LCMO. The Θ_1 values obtained from

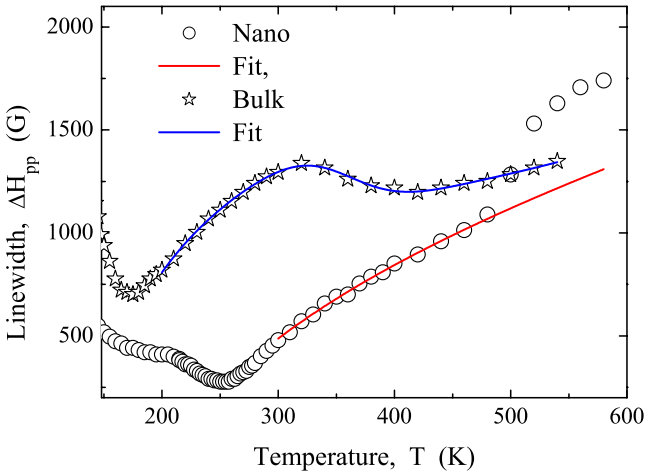

FIG. 9. (Color online) The same as in Fig. 8 for the linewidth ΔH_{pp} vs T dependences. Theoretical fits were done with Eqs. (3)–(5) and (2) as it is described in text. For nano LCMO the fitting curve is extended beyond T_0.

this fit agree excellently with the ones obtained previously using the temperature evolution of the DIN; see Tables I and II.

At $T>300$ K the ΔH_{pp} versus T dependence in the bulk is not monotonous; see Fig. 9. Numerical tests show that the broad minimum of ΔH_{pp} at $T\sim 420$ K is due to a peculiar form of the susceptibility described by Eq. (2). Therefore, Eq. (3) predicts such minimum even without the L_{e_g} term. However, taking this term into account improves the agreement between Eq. (3) and the experimental data. We performed the unconstrained fit of Eqs. (3)–(5), along with Eq. (2), to the data at 210 K$\leqslant T\leqslant$540 K assuming that ΔH_i^{∞}, B, and E_A are temperature independent. This seems quite reasonable for ΔH_i^{∞} as the variation of exchange (Θ) in bulk LCMO is indeed small, see Table I, but the assumption may not hold in the case of electronic parameters which can change upon the JT transition. The fit curve and the fit parameters are shown in Fig. 9 and in Table II, respectively. Except for σ_T, the parameters of Eq. (2) obtained from this fit agree excellently with those obtained from the fit to the DIN evolution, compare bulk sample sections in Tables I and II. The discrepancy in σ_T may be due the some changes of the parameters B and E_A with temperature.

IV. CONCLUSIVE REMARKS

The results obtained in this paper allow us to conclude the following. Bulk LCMO demonstrates well pronounced orthorhombic distortions, which according to the literature criterion,[17,26] are characteristic for stoichiometric low-doped $La_{1-x}Ca_xMnO_3$. In the LCMO nanocrystals the orthorhombic distortions are strongly reduced and structural O^*-O' transition is absent; see Fig. 1. However, we do not consider the suppression of the lattice transition part of JT effect as an evidence of nonstoichiometry following the above cited criterion.[17,26] We suggest that the main reason for the suppression of the lattice transition is a high degree of electron delocalization and virtual absence of long-living JT Mn^{3+} ions in the nanocrystals. Another reason may be the lattice compression due to a uniform strain induced by the enhanced surface effects. Thus the JT effect in the nano LCMO strongly influences the electron spectrum what manifests itself in EPR intensity and linewidth, but induces lattice distortions, which are insufficient for the structural transition. In a contrast, EPR probing of bulk LCMO reveals smeared cooperative JT transition; see Figs. 7(b), 8, and 9.

These facts strongly support our claim that the Ca-dopant distribution nonuniformity[43] smears the structural transition in the bulk LCMO, manifesting itself in DIN^{-1} versus T dependence modeled by Eq. (2). The mesoscale chemical disorder and structural imperfections in the bulk LCMO may lead to a partial depletion and confinement of holes in some regions of the crystal. The bulk is characterized by reduced Θ_{DE}, as compared to the maximum one attainable for Zener carriers,[5,6] large ΔH_i^{∞} and the Arrenius-type electronic contribution to ΔH_{pp}; see Tables I and II. All these features are unambiguous signatures of both holes depletion and binding.[5] The binding results in the formation of FM clusters embedded in AFM correlated matrix, detected in Refs. 14 and 15 and in this work. It should be emphasized that such phase coexistence in the bulk is induced by the chemical and structural disorder and has nothing in common with PS predicted by the idealized models.[2–4] On the contrary, a perfect chemical homogeneity and crystallinity of the nano LCMO lead to a predominantly bandlike propagation of e_g electrons, which maximizes the DE and makes the FM ground state feasible. This scenario is confirmed by the value of Θ_{DE} below JT transition, which is typical for the band electrons,[5,6] by nonactivated linearly changing with temperature contribution to ΔH_{pp} (Ref. 28) and by the reduced value of ΔH_i^{∞}; see Tables I and II. The strong contribution of surface effects results in the appearance of a SPM like phase in nanocrystals far above T_C.

The PM value of the g factor in the bulk and nano LCMO proves that for spatial and temporal scales accessible by EPR technique, the manganese ions are predominantly in the Mn^{4+} state (for a direct confirmation of the actual value of

TABLE II. The parameters of fits for the EPR linewidth. Spin dynamics parameters are the following: ΔH_i^{∞} is a high temperature asymptote of Mn^{4+} spin-spin relaxation contribution; B is a parameter of interaction between e_g electrons and impurities with spin reversal and E_A is the activation energy as described in the text.

Sample	ΔH_i^{∞} (G)	B (G K^{-1})	E_A (meV)	Θ_1 (K)	Θ_2 (K)	C_2/C_1	T_0 (K)	σ_T (K)
Nano	1318±211	1.25±0.38	0	214±6	Not involved in this fit			
Bulk	1785±70	148±6	375±12	137±2	141±14	1.29±0.05	363±5	49±5

Mn^{4+} ions' PM g factor; see, e.g., Ref. 47). It means that the site occupation picture does not apply to the majority of e_g electrons. This conclusion agrees well with the idea of a bond-centered occupation proposed for $La_{0.86}Sr_{0.14}MnO_3$.[48] A similar conclusion was drawn from the refinement of the neutron diffraction data for $Pr_{0.6}Ca_{0.4}MnO_3$ single crystal.[49] In addition, the domination of Mn^{4+} ions in magneto-optical activity was reported for $La_{0.925}Sr_{0.075}MnO_3$.[50] On the base of the above findings and our own results,[47,51] we suggest that in nano LCMO e_g electrons of former Mn^{3+} ions move bandlike and experience strong phonon-polaron effect, which results in shrinking of the e_g band above T_0. Therefore, no cooperative JT lattice distortion occurs in the nano LCMO due to the pronounced electron itinerancy. In bulk LCMO e_g electrons are also separated from the manganese sites but they are localized in clusters, which involve only few Mn^{4+} ions, due to concurrence of the extrinsic effects, such as doping inhomogeneity and crystalline defects, and the DE interactions. We suggest that the lifetime of Mn^{3+} ions in the nano LCMO is set by an intersite tunneling time of a band electron, while Mn^{3+} lifetime in the bulk, although longer than in the nanocase, is still shorter than the characteristic time of an EPR experiment. The observation of the cooperative JT distortions in the bulk, Fig. 1(b), may be seen as resulting from the confinement of e_g electrons in clusters containing some adjacent MnO_6 complexes in which intermediate valences of Mn ions occur.[49] As discussed above, the extrinsic imperfections in the bulk lead to the essential smearing of this JT transition.

The closeness of the ratios of the Curie constants above and below JT transition in the bulk and nano LCMO crystals, Table I, shows that the band width in both types of samples changes in the same manner. Namely, the concentration of e_g electrons and Mn^{4+} ions are the same in both types of samples. The linearity of the Curie constant in the carrier concentration has been theoretically demonstrated in the frame of a DE model.[52] Moreover, the closeness of the very Curie-Weiss temperatures in the bulk, below and above JT transition, and in the nanosample above JT transition, Table I, also points out to the same general mechanisms as being responsible for the magnetic ordering. These facts are the clear hallmarks of the same oxygen stoichiometry in addition to the same cation composition, which allowing us to claim that the observed change in electronic/magnetic ordering *is an inherent property* of LCMO. The difference in the magnetic ground state between the bulk and nanoform of LCMO crystals appears as a result of a size reduction down to nanometer scale and improved chemical homogeneity and crystallinity due to different fabrication method.

To conclude, we propose a *realistic model of the chemical/magnetic disorder suppression associated with the size reduction in doped manganites* using the representative example of the bulk and nanocrystalline $La_{09}Ca_{0.1}MnO_3$. The data presented in this work evidence that structural imperfections and chemical disorder play a dominant role in the coexistence of different magnetic/electronic phases and are capable of modifying significantly the phase diagram of the mixed valence manganites.

ACKNOWLEDGMENTS

This research was supported by the Israeli Science Foundation administered by the Israel Academy of Sciences and Humanities (Grant No. 845/05) and by the Israeli-Korean bilateral Grant No. 3-2217. S.S.B. acknowledges support by Grant No. AOARD-064054. The authors thank Yudith Grinblat for her assistance in HRTEM measurements.

*Corresponding author. evgenyr@bgu.ac.il

[1] *Colossal Magnetoresistance Oxides*, edited by Y. Tokura (Gordon and Breach, New York, 2000).
[2] E. Dagotto, *Nanoscale Phase Separation and Colossal Magnetoresistance*, Springer Series in Solid State Physics Vol. 136 (Springer-Verlag, Berlin, Heidelberg, 2003).
[3] J. Burgy, A. Moreo, and E. Dagotto, Phys. Rev. Lett. **92**, 097202 (2004).
[4] K. H. Ahn, T. Lookman, and A. R. Bishop, Nature (London) **428**, 401 (2004).
[5] M. Auslender and E. Kogan, Phys. Rev. B **65**, 012408 (2001).
[6] F. Popescu, C. Şen, and E. Dagotto, Phys. Rev. B **73**, 180404(R) (2006).
[7] C. Şen, G. Alvarez, and E. Dagotto, Phys. Rev. Lett. **98**, 127202 (2007).
[8] M. Fäth, S. Freisem, A. A. Menovsky, Y. Tomioka, J. Aarts, and J. A. Mydosh, Science **285**, 1540 (1999).
[9] M. Uehara, S. Mori, S. H. Chen, and S.-W. Cheong, Nature (London) **399**, 560 (1999).
[10] D. D. Sarma, D. Topwal, U. Manju, S. R. Krishnakumar, M. Bertolo, S. La Rosa, G. Cautero, T. Y. Koo, P. A. Sharma, S.-W. Cheong, and A. Fujimori, Phys. Rev. Lett. **93**, 097202 (2004).
[11] T. Becker, C. Streng, Y. Luo, V. Moshnyaga, B. Damaschke, N. Shannon, and K. Samwer, Phys. Rev. Lett. **89**, 237203 (2002).
[12] V. Moshnyaga, L. Sudheendra, O. I. Lebedev, S. A. Köster, K. Gehrke, O. Shapoval, A. Belenchuk, B. Damaschke, G. van Tendeloo, and K. Samwer, Phys. Rev. Lett. **97**, 107205 (2006).
[13] G. Van Tendeloo, O. I. Lebedev, M. Hervieu, and B. Raveau, Rep. Prog. Phys. **67**, 1315 (2004).
[14] G. Biotteau, M. Hennion, F. Moussa, J. Rodriguez-Carvajal, L. Pinsard, A. Revcolevschi, Ya. M. Mukovskii, and D. Shulyatev, Phys. Rev. B **64**, 104421 (2001).
[15] P. Kober-Lehouelleur, F. Moussa, M. Hennion, A. Ivanov, L. Pinsard-Gaudart, and A. Revcolevschi, Phys. Rev. B **70**, 144409 (2004).
[16] G.-L. Liu, J.-S. Zhou, and J. B. Goodenough, Phys. Rev. B **70**, 224421 (2004).
[17] M. Pissas, I. Margiolaki, G. Papavassiliou, D. Stamopoulos, and D. Argyriou, Phys. Rev. B **72**, 064425 (2005).
[18] P. A. Algarabel, J. M. De Teresa, J. Blasco, M. R. Ibarra, Cz. Kapusta, M. Sikora, D. Zajac, P. C. Riedi, and C. Ritter, Phys. Rev. B **67**, 134402 (2003).
[19] K. A. Yates, L. F. Cohen, C. Kapusta, P. C. Riedi, and L. Ghivelder, J. Magn. Magn. Mater. **260**, 105 (2003).
[20] R. H. Kodama, J. Magn. Magn. Mater. **200**, 359 (1999).
[21] X. Batlle and A. Labarta, J. Phys. D **35**, R15 (2002).

[22] S. S. Rao, K. N. Anuradha, S. Sarangi, and S. V. Bhat, Appl. Phys. Lett. **87**, 182503 (2005).
[23] S. S. Rao, S. Tripathi, D. Pandey, and S. V. Bhat, Phys. Rev. B **74**, 144416 (2006).
[24] N. Das, P. Mondal, and D. Bhattacharya, Phys. Rev. B **74**, 014410 (2006).
[25] V. A. Ivanshin, J. Deisenhofer, H.-A. Krug von Nidda, A. Loidl, A. A. Mukhin, A. M. Balbashov, and M. V. Eremin, Phys. Rev. B **61**, 6213 (2000).
[26] M. Pissas and G. Papavassiliou, J. Phys.: Condens. Matter **16**, 6527 (2004).
[27] D. L. Huber, G. Alejandro, A. Caneiro, M. T. Causa, F. Prado, M. Tovar, and S. B. Oseroff, Phys. Rev. B **60**, 12155 (1999).
[28] V. F. Gantmakher and Y. B. Levinson, *Carrier Scattering in Metals and Semiconductors* (North-Holland, Amsterdam, 1987).
[29] M. Auslender and E. Kogan, Eur. Phys. J. B **19**, 525 (2001).
[30] D. Shulyatev, S. Karabashev, A. Arsenov, and Ya. Mukovskii, J. Cryst. Growth **198/199**, 511 (1999).
[31] G. Pang, X. Xu, V. Markovich, S. Avivi, O. Palchik, Yu. Koltypin, G. Gorodetsky, Y. Yeshurun, H. P. Buchkremer, and A. Gedanken, Mater. Res. Bull. **38**, 11 (2003).
[32] J. B. Goodenough, in *Handbook on the Physics and Chemistry of Rare Earths*, edited by K. A. Gscheidner, Jr., J.-C. G. Bunzli, and V. K. Pecharsky (Elsevier Science B. V., New York, 2003), Vol. 33, Chap. 214.
[33] J. Rodriquez-Carvajal, Physica B **192**, 55 (1992).
[34] A. I. Shames, E. Rozenberg, W. H. McCarroll, M. Greenblatt, and G. Gorodetsky, Phys. Rev. B **64**, 172401 (2001).
[35] T. Ji, J. Fang, V. Golob, J. Tang, and Ch. J. O'Connor, J. Appl. Phys. **92**, 6833 (2002).
[36] B. B. Van Aken, O. D. Jurchescu, A. Meetsma, Y. Tomioka, Y. Tokura, and T. T. M. Palstra, Phys. Rev. Lett. **90**, 066403 (2003).
[37] G. Alejandro, M. C. G. Passeggi, D. Vega, C. A. Ramos, M. T. Causa, M. Tovar, and R. Senis, Phys. Rev. B **68**, 214429 (2003).
[38] M. T. Causa, M. Tovar, A. Caneiro, F. Prado, G. Ibanez, C. A. Ramos, A. Butera, B. Alascio, X. Obradors, S. Pinol, F. Rivadulla, C. Vazquez-Vazquez, A. Lopez-Quintela, J. Rivas, Y. Tokura, and S. B. Oseroff, Phys. Rev. B **58**, 3233 (1998).
[39] V. Chechersky, A. Nath, S. E. Lofland, S. Newlander, L. Cerquoni, Y. Mukovskii, A. A. Arsenov, G. Karabshev, D. A. Shulyatev, and R. L. Greene, Phys. Rev. B **63**, 214401 (2001).
[40] P. Dey and T. K. Nath, Phys. Rev. B **73**, 214425 (2006).
[41] J. C. Slonczewski, Phys. Rev. B **39**, 6995 (1989).
[42] C. Ritter, M. R. Ibarra, J. M. De Teresa, P. A. Algarabel, C. Marquina, J. Blasco, J. García, S. Oseroff, and S.-W. Cheong, Phys. Rev. B **56**, 8902 (1997).
[43] D. Shulyatev, S. Karabashev, A. Arsenov, Ya. M. Mukovskii, and S. Zverkov, J. Cryst. Growth **237/239**, 810 (2002).
[44] I. Dzialoshinsky, J. Phys. Chem. Solids **4**, 241 (1958).
[45] T. Moriya, Phys. Rev. Lett. **4**, 228 (1960); Phys. Rev. **120**, 91 (1960).
[46] J. B. Goodenough, *Magnetism and the Chemical Bond* (Interscience, New York, 1963).
[47] A. I. Shames, M. Auslender, E. Rozenberg, G. Gorodetsky, S. Hébert, and C. Martin, J. Magn. Magn. Mater. **316**, e640 (2007).
[48] J.-S. Zhou and J. B. Goodenough, Phys. Rev. B **62**, 3834 (2000).
[49] A. Daoud-Aladine, J. Rodriguez-Carvajal, L. Pinsard-Gaudart, M. T. Fernandez-Diaz, and A. Revcolevschi, Phys. Rev. Lett. **89**, 097205 (2002).
[50] E. A. Balykina, E. A. Ganshina, G. S. Krinchik, A. Yu. Trifonov, and I. O. Troyanchuk, J. Magn. Magn. Mater. **117**, 259 (1992).
[51] A. I. Shames, M. Auslender, E. Rozenberg, G. Gorodetsky, C. Martin, and A. Maignan, J. Appl. Phys. **97**, 10H704 (2005).
[52] R. S. Fishman and M. Jarrell, Phys. Rev. B **67**, 100403(R) (2003).